Bile salt–dependent lipase interacts with platelet CXCR4 and modulates thrombus formation in mice and humans

Laurence Panicot-Dubois,[1,2] Grace M. Thomas,[2] Barbara C. Furie,[1] Bruce Furie,[1] Dominique Lombardo,[2] and Christophe Dubois[1,2]

[1]Division of Hemostasis and Thrombosis, Department of Medicine, Beth Israel Deaconess Medical Center and Harvard Medical School, Boston, Massachusetts, USA. [2]INSERM UMR 911, Université de la Méditerranée, Faculté de Médecine — Timone, Marseille, France.

Bile salt–dependent lipase (BSDL) is an enzyme involved in the duodenal hydrolysis and absorption of cholesteryl esters. Although some BSDL is transported to blood, the role of circulating BSDL is unknown. Here, we demonstrate that BSDL is stored in platelets and released upon platelet activation. Because BSDL contains a region that is structurally homologous to the V3 loop of HIV-1, which binds to CXC chemokine receptor 4 (CXCR4), we hypothesized that BSDL might bind to CXCR4 present on platelets. In human platelets in vitro, both BSDL and a peptide corresponding to its V3-like loop induced calcium mobilization and enhanced thrombin-mediated platelet aggregation, spreading, and activated $\alpha_{IIb}\beta_3$ levels. These effects were abolished by CXCR4 inhibition. BSDL also increased the production of prostacyclin by human endothelial cells. In a mouse thrombosis model, BSDL accumulated at sites of vessel wall injury. When CXCR4 was antagonized, the accumulation of BSDL was inhibited and thrombus size was reduced. In BSDL$^{-/-}$ mice, calcium mobilization in platelets and thrombus formation were attenuated and tail bleeding times were increased in comparison with those of wild-type mice. We conclude that BSDL plays a role in optimal platelet activation and thrombus formation by interacting with CXCR4 on platelets.

Introduction

Pancreatic cholesterol esterase or bile salt–dependent lipase (BSDL; E.C.3.1.1.13) is an enzyme involved in the duodenal hydrolysis and absorption of cholesteryl esters (1, 2). BSDL is synthesized in the endoplasmic reticulum of pancreatic acinar cells and follows the secretion pathway to the duodenal lumen (3). The enzyme, which is N- and O-glycosylated (4, 5), is found in pancreatic secretions of all vertebrates examined to date. To generate significant lipase activity, BSDL must interact with bile salts in the duodenal lumen. Once activated, BSDL, in concert with other digestive lipolytic enzymes, degrades dietary lipids and participates in the hydrolysis of cholesterol esters into free cholesterol and fatty acids (6). In the duodenum, a fraction of BSDL is internalized by enterocytes via the lectin-like oxidized LDL receptor (LOX-1) and transported to the blood compartment (7, 8), where it partly associates with apolipoprotein B–containing lipoproteins in plasma (6). The concentration of circulating BSDL in human serum, determined by ELISA using polyclonal antibodies, is 1.5 ± 0.5 μg/l (9–11) but is elevated to a level as high as 7 μg/l in some pathological conditions, such as acute pancreatitis (12). BSDL has also been detected in human aortic homogenate and in atherosclerotic lesions of hypercholesterolemic monkeys and of human arteries (13). This enzyme is also found in the vessel wall homogenate (14). Although there are conflicting reports, the enzyme may be synthesized by macrophages and endothelial cells (14, 15). Alternatively, BSDL, which has a heparin-binding site (16) and a V3-like loop domain (17), associates with intestinal cell-surface proteoglycans (7, 8). In vitro studies have shown that BSDL induces vascular smooth muscle cell proliferation and evokes endothelial cell proliferation and chemotactic migration (13, 18). However, the function of circulating plasma pancreatic BSDL is still unknown.

Platelets, in addition to their role in hemostasis, are involved in inflammation, immunological reactions, and atherosclerosis. Platelets contain both chemokine receptors expressed at their surfaces and chemokines, such as RANTES and MIP-1, stored in platelet granules and released upon platelet activation (19, 20). In particular macrophage-derived chemokine (MDC), which is not present in platelet granules, and stromal cell–derived factor–1 (SDF-1), which may be present in platelet granules (19, 21), have been described as platelet agonists by interacting with CCR4 and CXCR4, respectively. SDF-1 binding to CXCR4 induces intracellular calcium mobilization in platelets and increases platelet aggregation induced by thrombin or ADP (22, 23). The ability of chemokines to stimulate platelets is dependent upon the presence of platelet agonists such as ADP or thrombin (24). Furthermore, chemokine-induced platelet aggregation is inhibited by aspirin, suggesting involvement of thromboxane A_2 in this response (25).

CXCR4 interacts with the V3 loop of the 120-kDa glycoprotein (gp120) from HIV-1 (26). Since BSDL contains a structure homologous to this V3 loop, called the V3-like loop domain (17) (amino acid residues N361 to L393; Table 1), we explored the interaction of circulating BSDL with the platelet CXCR4 receptor. We have determined that BSDL is stored in platelets and released upon platelet activation. Furthermore, circulating BSDL and/or BSDL released from platelets play a significant synergistic role in optimal platelet activation and thrombus formation through its action on platelet CXCR4.

Nonstandard abbreviations used: BSDL, bile salt–dependent lipase; CXCR4, CXC chemokine receptor 4; FAPP, fetoacinar pancreatic protein; hBSDL, human BSDL; mBSDL, mouse BSDL; SDF-1, stromal cell–derived factor–1; TRAP-1, thrombin receptor activation peptide 1.

Conflict of interest: The authors have declared that no conflict of interest exists.

Citation for this article: *J. Clin. Invest.* **117**:3708–3719 (2007). doi:10.1172/JCI32655.

Table 1
Amino acid composition of peptides related to the sequence of the V3-like loop domain of BSDL

Peptide	aa composition
V3	NATYEVYTEPWAQDSSQETRKKTMVDLETDIL
V3Lscr	NLAITDYTEEVLYDTVEMPTWKAKQRDTSESQ[A]
V3Lsal	NATYEVYTEPAAQDSSQETAKATMVDLETDIL[B]

[A]The scrambled peptide has the same amino acid composition as the V3-like peptide but differs in sequence. [B]Mutations are underlined.

Results

Purified BSDL acts as a chemokine on platelets. SDF-1, a known CXCR4 ligand, does not induce platelet aggregation by itself but increases platelet aggregation induced by thrombin or ADP (Table 2) (23). We determined whether human BSDL (hBSDL), with its V3-like loop, can modulate platelet aggregation induced by different agonists. Purified hBSDL (27) had no effect on resting platelets. However the presence of BSDL significantly enhanced activation of platelets by suboptimal concentrations of thrombin (Figure 1, A and B). A similar effect of hBSDL was observed using 2.5 μM ADP and Par1 and Par4 agonist peptides SFLLRN (thrombin receptor activation peptide–1 [TRAP-1] at 10 μM) and AYPGKF (TRAP-4 at 100 μM) in place of thrombin (Table 2). At 0.8 U/ml of thrombin, a 5% increase in aggregation was observed when BSDL was included (Figure 1A, right panel). At 0.5 U/ml of thrombin, a 15% increase in aggregation was observed with hBSDL (Figure 1A, middle panel). At 0.1 U/ml of thrombin, a 75% increase was observed in the presence of hBSDL (Figure 1A, left panel, and Figure 1B). The effect of BSDL on thrombin-induced platelet aggregation was blocked by the inhibitory antibody against CXCR4, 12G5, thus indicating a role for CXCR4 in this process. To determine whether hBSDL augments thrombin-induced platelet aggregation through interaction between its V3-like loop and CXCR4 on platelets, we performed experiments using V3-like loop peptides (Table 1), CXCR4-blocking antibodies (clone 12G5 and clone 44716.111), or a specific CXCR4 antagonist (AMD3100) (28). Addition of 1 μg of V3-like loop domain peptide (Table 1, V3) to thrombin-activated platelets augmented aggregation similarly to hBSDL (Figure 1B). In contrast, a V3-like loop peptide mutated at amino acids involved in the salt bridge or with a scrambled sequence (Table 1, V3LSal, V3Lscr) did not increase platelet aggregation (Figure 1B). In the presence of CXCR4-blocking antibodies (12G5) (Figure 1A) or the CXCR4 antagonist, but not in the presence of irrelevant control antibody (data not shown), BSDL and the V3-like loop peptide had no effect on thrombin-induced platelet aggregation (Figure 1B).

hBSDL also influences platelet spreading. Although BSDL had no effect on resting human platelets, it increased the spreading of thrombin-activated platelets on a glass coverslip after 20 and 40 minutes (Figure 2, A and B). Platelet aggregation and spreading are both mediated by intracellular signaling, converging on the activation of the integrin $\alpha_{IIb}\beta_3$. The extent of $\alpha_{IIb}\beta_3$ activation in thrombin-activated platelets significantly increased in the presence of hBSDL (Figure 2C), but there was no effect of hBSDL on P selectin surface expression of thrombin-activated platelets (data not shown). Thus, hBSDL does not increase the magnitude of degranulation but only the magnitude of $\alpha_{IIb}\beta_3$ activation. Addition of the V3-like loop domain peptide also augmented thrombin-induced $\alpha_{IIb}\beta_3$ activation, but the mutated V3-like loop domain peptide and the scrambled V3-like peptide did not (Figure 2C). The effects of BSDL or V3 peptide were blocked when platelets were treated with 1 mM aspirin (data not shown), suggesting that production of thromboxane A_2 plays a key role in the intracellular pathways induced by BSDL on platelets.

Previous reports have shown that the binding of SDF-1 to platelet CXCR4 induces calcium mobilization (25). We demonstrated that BSDL and the V3 loop peptide had a similar effect. When platelets were challenged with 0.5 μg BSDL or with 0.1 μg V3-like loop peptide, intracellular calcium was mobilized, as measured using fura-2. This calcium rise was blocked when CXCR4 was inhibited with the anti-CXCR4 antibody 12G5 (Figure 2D). These results indicate that purified hBSDL or the V3-like loop peptide act on CXCR4 to induce calcium mobilization, to enhance $\alpha_{IIb}\beta_3$ activation, to augment platelet aggregation, and to increase platelet spreading induced by thrombin.

BSDL is stored in platelets and released upon activation. To understand the mechanisms involved in the action of BSDL on activated platelets, we determined whether platelets contain or express BSDL. We observed that washed platelet lysates prepared from different individuals all specifically reacted by Western blotting at the same molecular mass as human purified BSDL (115 kDa) with the antibody pAbL32 directed against hBSDL (Figure 3A). Similar results were observed with the anti-BSDL antibody pAbL64 (data not shown). When platelets were activated with 0.1 U/ml thrombin and washed before lysis, the quantity of BSDL contained within platelets decreased in comparison with that in resting platelets (Figure 3B). As a control, we verified that the quantity of protein loaded before and after platelet activation was identical (42 μg of protein loaded in each well). These results were confirmed by FACS analysis. The signal corresponding to BSDL was increased in resting permeabilized platelets in comparison with nonpermeabilized or activated platelets (Figure 3C). The quantity of BSDL present in platelets was estimated by Western blot analysis as 6,000 molecules of BSDL per platelet. Kowalska et al. have previously estimated the quantity of CXCR4 expressed on resting human platelets as 2,600 receptors per platelet (22). We observed by immunofluorescence that the quantity of CXCR4 present on the platelet membrane increased following platelet activation by 0.1 U/ml thrombin (Figure 3D). Together,

Table 2
Effect of BSDL on platelet aggregation induced by different agonists

Conditions	Maximal % of platelet aggregation
10 μM TRAP-1	75% ± 8%
10 μM TRAP-1 + 5 μg BSDL	88% ± 5%
100 μM TRAP-4	66% ± 5 %
100 μM TRAP-4 + 5 μg BSDL	80% ± 8%
2.5 μM ADP + 240 μg/ml fibrinogen	28% ± 6%
2.5 μM ADP + 240 μg/ml fibrinogen + 5 μg BSDL	40% ± 5%
0.1 U/ml thrombin + 0.4 U apyrase	24% ± 7%
0.1 U/ml thrombin + 0.4 U apyrase + 5 μg BSDL	51% ± 6%
100 μM SDF-1	No aggregation
0.1 U/ml thrombin	40% ± 6%
0.1 U/ml thrombin + 100 μM SDF-1	72% ± 7%

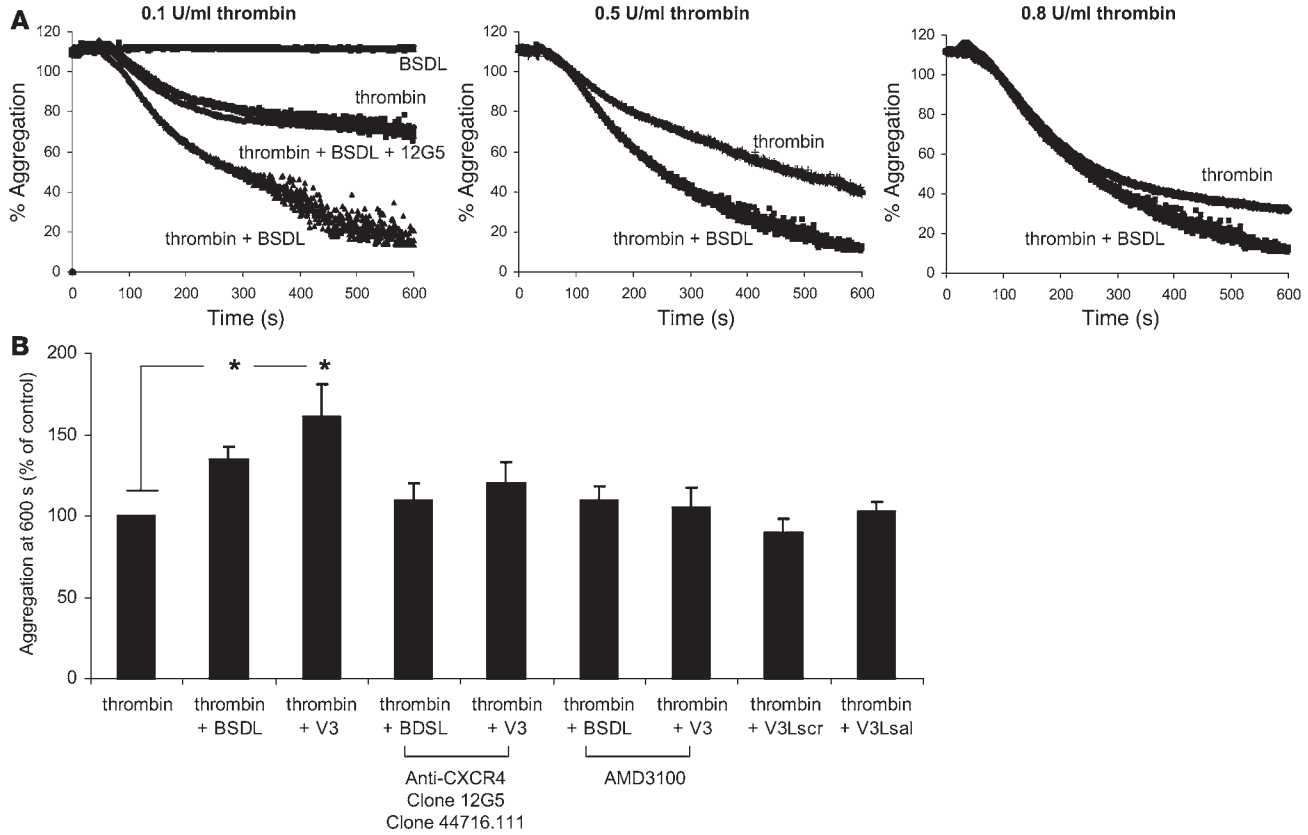

Figure 1

BSDL and V3-like loop peptides enhance platelet aggregation induced by thrombin. (**A**) Kinetics of platelet aggregation induced by 0.1 U/ml (left panel), 0.5 U/ml (middle panel), or 0.8 U/ml thrombin (right panel) in the absence or presence of 5 μg BSDL. (**B**) The extent of aggregation of platelets activated with 0.1 U/ml thrombin in the presence of BSDL (5 μg), V3, V3Lsrc, or V3Lsal peptides (1 μg) ($n = 10$; $^*P < 0.01$) is indicated as a percentage of platelet aggregation in the presence of 0.1 U/ml of thrombin alone. Where indicated, platelets were incubated with blocking anti-CXCR4 antibodies (clone 12G5 or clone 44716.111) or a CXCR4 antagonist (AMD3100) before addition of thrombin.

these results indicate that upon thrombin activation, platelets exposed more CXCR4 receptors at their surface. This would explain why BSDL and SDF-1 mainly act on activated platelets.

Endogenous BSDL accumulates at the site of laser-induced injury in living mice. To determine whether BSDL might play a physiological role in platelet aggregation and thrombus formation, we studied the biology of BSDL within the context of thrombus formation in a live mouse. We have previously described an in vivo model of thrombosis using intravital high-speed confocal and wide-field multichannel digital microscopy, which allows the detection in real time of fluorescence signals at the site of laser-induced injury in mice (29). Using polyclonal anti-hBSDL antibodies, pAbL32 and pAbL64, and pAbantipeptide (30), all cross-reactive with mouse BSDL (mBSDL), we determined that endogenous mBSDL accumulates in arterial thrombi in vivo following laser-induced vessel wall injury (31). Endogenous mBSDL accumulation at the site of injury could be detected using any of the 3 polyclonal antibodies. A representative example using pAbantipeptide is shown in Figure 4A. The median accumulation of the fluorescence signal corresponding to an antibody directed against endogenous BSDL (26 thrombi in 3 wild-type mice) versus an irrelevant antibody (36 thrombi in 3 wild-type mice) over time is shown in Figure 4B. BSDL-reactive antibodies, but not irrelevant antibody, were detected immediately after laser injury, and its signal increased over time in parallel with the developing thrombus. The same kinetics of BSDL accumulation were observed when polyclonal antibodies pAbL32 or pAbL64 were infused into the circulation of wild-type mice (32 thrombi in 3 mice for each antibody) with differences in the maximum integrated fluorescence intensity of the 2 antibodies (Figure 4C). These results indicate that following laser-induced injury, endogenous BSDL accumulates at the site of injury. Confocal intravital microscopy in real time was performed to localize endogenous BSDL relative to platelets within a developing thrombus (Figure 4D). Platelets were identified with fluorescently labeled Fab fragments derived from a monoclonal anti-CD41 antibody as previously described (32). Endogenous mBSDL (green) and platelets (red) colocalized (merge, yellow) in a focal plane through the approximate center of the thrombus, indicating that BSDL interacts with the vessel wall and platelets participating in a developing thrombus in vivo. Endothelial cells such as HUVECs have been previously described to express CXCR4 on their surfaces, and this expression could be increased following activation of endothelial cells (33). In vitro, hBSDL did not affect the production of nitric oxide (Figure 5A). However, the enzyme significantly increased HUVEC production of prostacyclin in a dose-dependent manner following treatment with 0.1 U/ml thrombin (Figure 5B). These results suggest that BSDL could also participate in the in vivo activation of the injured endothelium.

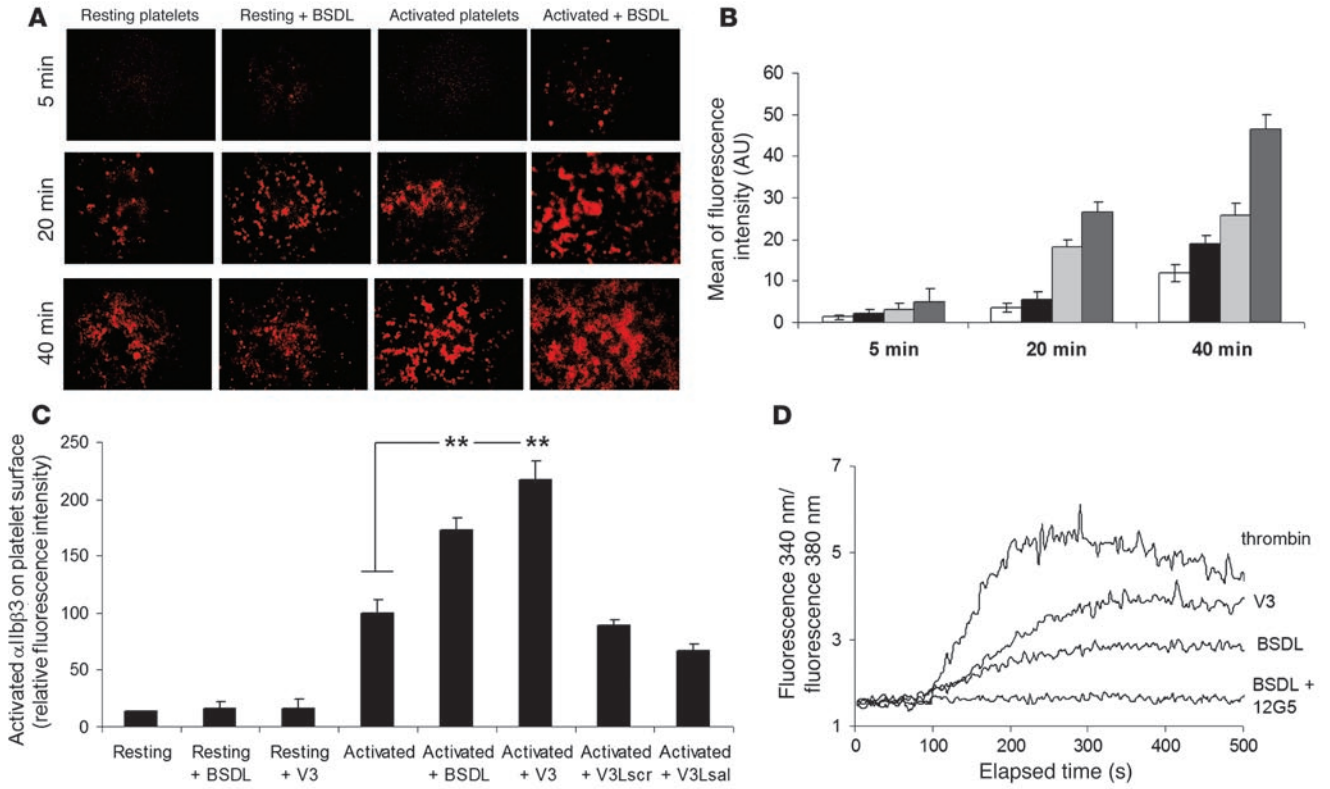

Figure 2

Effect of BSDL or V3-like loop peptides on platelet spreading and platelet activation. (**A**) Spreading of resting or thrombin-activated platelets treated with BSDL. Platelets were fluorescently labeled with Alexa Fluor 647–conjugated anti-mouse CD41 Fab fragment. Original magnification, ×600. (**B**) The mean fluorescence intensity of 15 representative microscopic fields of spread platelets at 3 time points after activation and addition of BSDL was calculated. White bars, resting platelets; black bars, resting platelets in the presence of hBSDL; light gray bars, thrombin-activated platelets; dark gray bars, thrombin-activated platelets in the presence of hBSDL. $^{**}P < 0.001$. (**C**) Fluorescence intensity of PAC-1 FITC-labeled antibodies (directed against activated $\alpha_{IIb}\beta_3$) bound to resting or thrombin-activated platelets in the presence or absence of human BSDL (5 μg), V3 peptide (1 μg), V3Lscr peptide (1 μg), or V3Lsal peptide (1 μg) ($n = 9$; $^{**}P < 0.001$). (**D**) Platelets were loaded with 3 μM fura-2/AM for 30 minutes at 37°C. Intracellular Ca^{2+} levels were monitored as the ratio of fluorescence emission intensity at 510 nm after excitation at 340 to that after excitation at 380 nm as described in Methods. Platelets were stimulated with 0.1 U/ml thrombin, 0.5 μg BSDL in the absence or presence of the blocking anti-CXCR4 antibody 12G5, or 0.1 μg/ml of V3 peptide.

Thrombus formation is defective in BSDL-null mice. The participation of BSDL in thrombus formation after laser injury was confirmed by studying thrombus formation in BSDL-null mice (34). As anticipated, no BSDL could be detected accumulating in the thrombus of BSDL-null mice (Figure 6A). The kinetics of platelet accumulation in wild-type mice and BSDL-null mice were compared (Figure 6B). By studying 30 thrombi and determining the median values as a function of time, we observed that while the kinetics of thrombus growth were similar in the 2 genotypes, thrombus size was reduced in BSDL-null mice in comparison with wild-type mice (Figure 6C). Peak platelet accumulation was reduced 50% in BSDL-null mice in comparison with wild-type mice (Figure 6D). When the maximal fluorescence intensities corresponding to platelet accumulation for each thrombus in BSDL-null ($n = 36$, 3 mice) and wild-type mice ($n = 32$, 3 mice) were ranked in order of increasing thrombus size and compared using quartile analysis, we observed that 8% of thrombi in BSDL-null mice but 47% of thrombi in wild-type mice constituted the largest thrombi (Figure 6E). These results confirm that maximal thrombus size was reduced in BSDL-null mice. However, there were no significant differences in the median time to maximum platelet accumulation after laser-induced injury between the 2 mouse genotypes (data not shown). These results suggest that BSDL enhances the activation and aggregation of platelets in vivo.

To confirm the involvement of endogenous BSDL in optimal thrombus formation, we examined tail vein bleeding time as a method of monitoring the kinetics of thrombus formation. The median tail vein bleeding time observed for BSDL-null mice was 395 seconds ($n = 10$), significantly higher than the 120-second median tail vein bleeding time for wild-type mice ($n = 10$) (Figure 7A). Together these in vivo results indicate that BSDL plays a role in optimal thrombus formation.

Platelet activation but not thrombin generation is diminished in vivo in BSDL-null mice. We have previously shown that thrombin is the major platelet agonist involved in thrombus formation following laser-induced injury under our conditions (35). To exclude the possibility that thrombin generation was defective in BSDL-null mice in comparison with wild-type mice, fibrin accumulation at the site of injury was compared in BSDL-null and wild-type mice. No differences were observed in fibrin generation at the site of laser-induced injury in BSDL-null ($n = 28$, 3 mice) and wild-type mice ($n = 30$, 3 mice) (Figure 7B). We conclude that BSDL plays

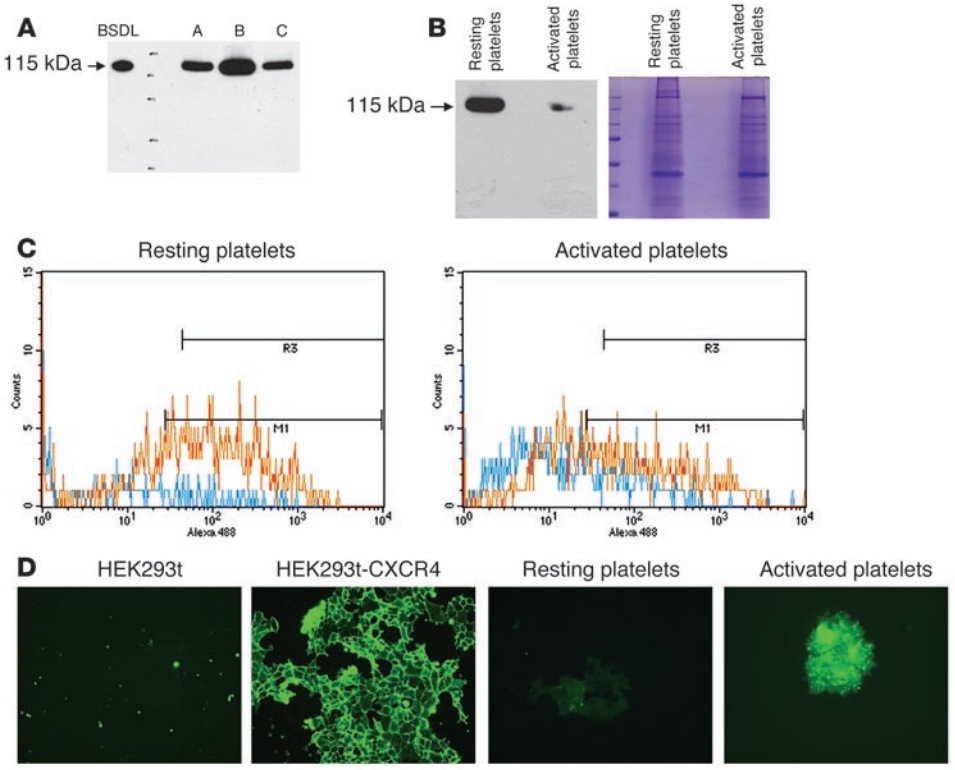

Figure 3
Human platelets contain BSDL. (**A**) Western blot analysis of washed platelet lysates (80 μg of protein/well) prepared from 3 different individuals using the anti-hBSDL antibody pAbL32. Purified hBSDL (2 ng) was loaded as a control. (**B**) Resting or thrombin-activated (0.1 U/ml) washed platelets were lysed and protein lysates loaded onto a polyacrylamide gel (42 μg of protein/well), separated by electrophoresis, and either transferred to a nitrocellulose membrane and revealed with the pAbL32 antibody (left) or stained with Coomassie blue (right). (**C**) Resting (left) or thrombin-activated platelets (0.1 U/ml; right) were analyzed by flow cytometry using the pAbL32 Alexa Fluor 480–conjugated antibody. Permeabilized platelets are depicted in red and nonpermeabilized platelets in blue. (**D**) Immunofluorescence of HEK293t cells (negative control), HEK293t cells transfected with CXCR4 (positive control), or resting or activated platelets using an antibody directed against CXCR4 (original magnification, ×200; $n = 3$).

a role in vivo in platelet thrombus growth without affecting thrombin generation.

We have recently described a method to monitor in vivo calcium mobilization in fura-2–loaded platelets participating in the development of a thrombus (36, 37). This method was used to compare in vivo platelet activation in BSDL-null mice and wild-type mice. Fura-2–loaded platelets (250×10^6 to 300×10^6) prepared from BSDL-null or wild-type mice were infused into the circulation of a donor mouse of the same genotype. Fura-2–loaded platelets were detected after excitation at 380 nm and emission at 510 nm. Calcium mobilization into these platelets was detected after excitation at 340 nm and emission at 510 nm as previously described (38). Whereas fura-2–loaded platelets (green) rapidly accumulated at the site of laser injury, calcium mobilization (in yellow) was reduced in BSDL-null mice in comparison with wild-type mice (Figure 8A). As previously observed by infusing antibodies directed against CD41, the maximal size of the thrombus was also reduced in the BSDL-null mice in comparison with the wild-type mice (Figure 8, A and B). Platelet activation was quantitated by analysis of the median fluorescence associated with calcium mobilization in multiple thrombi in wild-type ($n = 18$, 3 mice) and BSDL-null mice ($n = 18$, 3 mice) (Figure 8, B and C). To correct the magnitude of platelet activation for the decreased accumulation of platelets observed in BSDL-null mice compared with wild-type mice (Figure 8B), the mean integrated fluorescence associated with activated platelets was compared with the mean integrated fluorescence associated with the total platelets accumulated within the thrombus (Figure 8C). In this analysis, platelet activation, as measured by the ratio of fluorescence associated with activated platelets to the fluorescence associated with total platelets, was diminished by 50% in BSDL-null mice in comparison with wild-type mice. These results indicate that although fibrin generation is equivalent in BSDL-null mice and wild-type mice, activation of BSDL-null platelets is defective in this in vivo model. These results indicate that in vivo blood BSDL plays a role in platelet activation leading to optimal thrombus formation.

In vivo blocking of CXCR4 inhibits BSDL accumulation and reduced thrombus formation. Our in vitro results indicate that purified BSDL interacts with CXCR4 on human platelets. To determine whether in vivo endogenous mBSDL is involved in optimal platelet activation by interacting with CXCR4 on platelet and endothelial cells, we compared the kinetics of endogenous mBSDL and platelet accumulation in wild-type mice in the presence of the CXCR4 antagonist AMD3100 or in the presence of the vehicle alone (28). The specific CXCR4 antagonist AMD3100 prevented the binding of endogenous BSDL and markedly reduced accumulation of platelets at the site of laser injury (Figure 9, A and B), confirming that the interaction of BSDL with CXCR4 on platelets and the endothelium impacts thrombus formation in vivo.

Discussion

Blood coagulation is a host defense mechanism that maintains the closed circulatory system when blood vessel integrity is compromised. Pathological processes such as inflammation and atherosclerosis are associated with thrombosis. Thrombosis is also a major complication in gastrointestinal adenocarcinoma, particularly pancreatic carcinoma (39). In addition to BSDL, pancreatic carcinoma cells express high levels of an oncofetal variant of the enzyme, the fetoacinar pancreatic protein (FAPP) (40, 41), missing 10 of 16 proline-rich repeats at the C-terminal end of the protein but containing the V3-like loop region (42). This protein is found at elevated levels in most patients with pancreatic cancer (40). We thus sought to define the role of circulating BSDL.

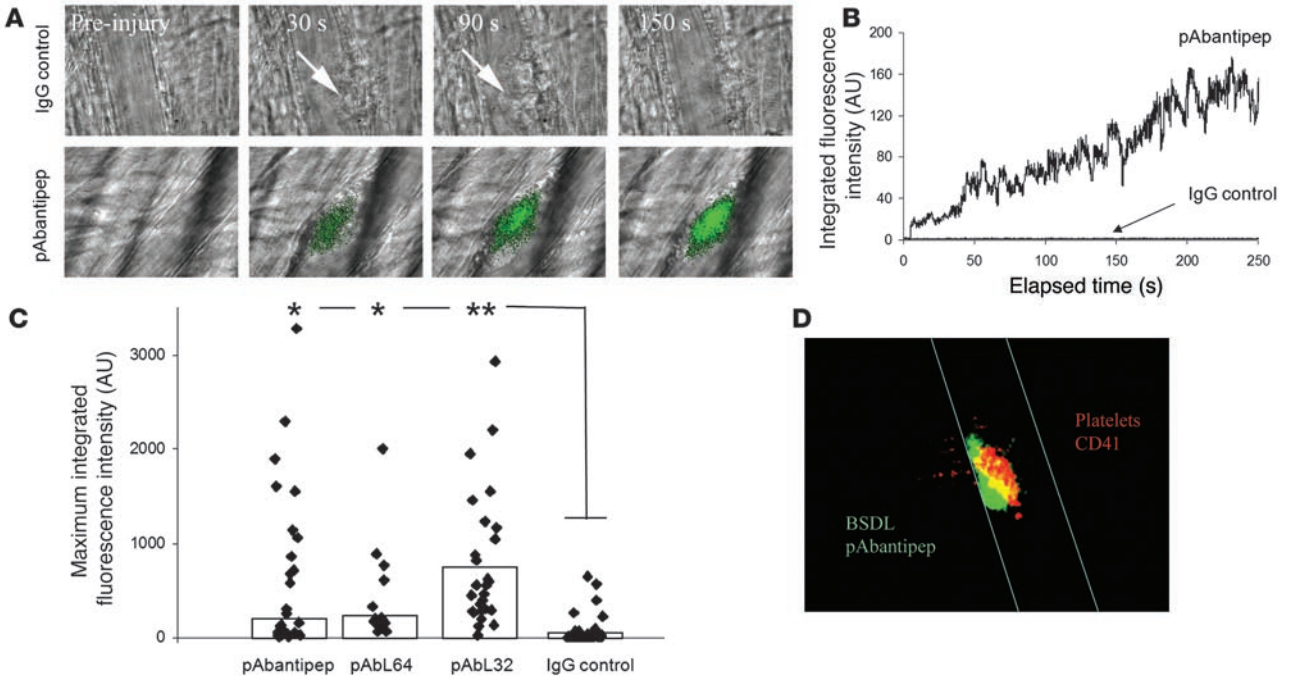

Figure 4

Endogenous mBSDL accumulates at sites of injury in vivo. (**A**) Wild-type mice were infused with the rabbit polyclonal pAbantipeptide (pAbantipep) antibodies (0.6 μg/g mouse) (26 thrombi, 3 mice) or with an irrelevant rabbit IgG (IgG control; 1 μg/g mouse weight) (36 thrombi, 3 mice) and Alexa Fluor 488–conjugated goat anti-rabbit antibody (0.6–1 μg/g of mouse). A fluorescence signal corresponding to the accumulation of pAbantipeptide antibodies (green), but not the irrelevant antibody, was detected at the site of thrombus formation after laser-induced injury. Arrows indicate the site of thrombus formation in mouse receiving the irrelevant rabbit IgG. Original magnification, ×600. (**B**) Median integrated BSDL fluorescence intensity as a function of time (s) in wild-type mice after laser injury to the arteriolar vessel wall following infusion of rabbit polyclonal antibodies pAbantipeptide (0.6 μg/g mouse; 26 thrombi, 3 mice) or IgG control (1 μg/g mouse; 36 thrombi, 3 mice). (**C**) The maximum fluorescence intensities for each thrombus obtained after infusion of pAbantipeptide (26 thrombi, 3 mice), pAbL64 (15 thrombi, 3 mice), pAbL32 (32 thrombi, 4 mice), or IgG control (36 thrombi, 3 mice) in wild-type mice are plotted. The bars indicate the median maximum fluorescent intensity for each antibody. $^{*}P < 0.01$; $^{**}P < 0.001$ (**D**) Representative image of endogenous BSDL (green) and platelets (red) colocalized (yellow) in a growing thrombus observed by intravital confocal microscopy. Original magnification, ×600.

In this study we demonstrate that BSDL plays a physiological role in thrombus formation, a unique function for a lipase. Our in vitro results indicate that BSDL, by increasing the amount of activated $\alpha_{IIb}\beta_3$, enhances both the aggregation and the spreading of thrombin-activated platelets. The enzyme also induces calcium mobilization, a marker of platelet activation. The V3-like loop structure of BSDL mimics these effects through interaction with the chemokine receptor CXCR4. In vivo, we show that BSDL accumulates in a CXCR4-dependent interaction on platelets at the site of laser-induced injury, enhancing platelet accumulation. These results indicate that BSDL acts as a chemokine to optimize platelet aggregation and platelet thrombus formation.

There have been several studies on the effects of chemokines on platelets in vitro (19, 20, 24). Based on the action of SDF-1 on platelets, some chemokines have been defined as weak platelet agonists (25) because of the increased platelet aggregation induced by thrombin or ADP after chemokine stimulation. Furthermore Clemetson et al. (19) have shown that SDF-1 induces intracellular calcium mobilization in platelets. These effects are prevented when the production of thromboxane A_2 is inhibited by aspirin. In the present study, we observed that BSDL or a peptide with sequence homology to its V3-like loop induces calcium mobilization and increases platelet aggregation and $\alpha_{IIb}\beta_3$ activation in thrombin-activated platelets. These effects were prevented using either blocking antibodies or a specific inhibitor (AMD3100) against CXCR4 or aspirin to prevent the generation of thomboxane A_2. Based on our results and those described for chemokines (25), we conclude that BSDL acts as a chemokine on platelets.

Two studies have previously determined the concentration of circulating BSDL in serum at 1.5 ± 0.5 μg/l (9, 11). We have previously shown that BSDL is found in the circulation both free and bound to apolipoprotein B–containing lipoproteins (7). Further analysis of the original data allowed us to calculate the distribution of free BSDL versus BSDL bound to apolipoprotein B–containing lipoproteins bound BSD. We determined that 35% ± 7% of the total circulating BSDL was found free in plasma versus 57% ± 7% bound to apolipoprotein B–containing lipoproteins (VLDL, LDL, and chylomicrons). However, we present here evidence that BSDL is also detectable in platelets and released into the blood circulation upon activation. It is then possible that the quantity of local BSDL increases greatly during the formation of a platelet thrombus. This explains why we can detect endogenous BSDL at sites of laser-induced injury (Figure 3). Therefore, we conclude that in vivo, the local concentration of BSDL at the sites of injury is much higher than the concentration of circulating BSDL in blood. Although some BSDL is associated with platelets within the thrombus, some also concentrates

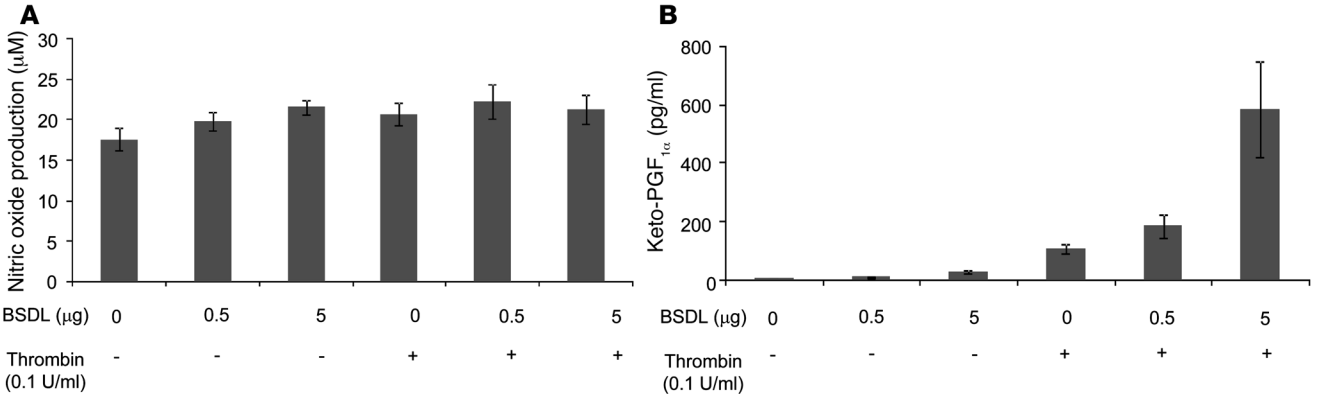

Figure 5
BSDL induces in vitro the production of prostacyclin by HUVECs. HUVECs were cultured as described in Methods and challenged with different amounts of purified BSDL in the absence (–) or presence (+) of 0.1 U/ml thrombin for 6 hours. The production of nitric oxide (**A**) and prostacyclin (**B**) was determined as described in Methods (n = 3).

on the vessel wall. Since in vitro studies have shown that BSDL can interact with activated endothelial cells to promote wound healing, we determined whether BSDL could modify the prostacyclin and nitric oxide production of HUVECs in vitro. Our results showed that indeed BSDL increases the production of prostacyclin by thrombin-treated HUVECs. This may explain why in vivo a fraction of detected BSDL was interacting with (activated) endothelium at the site of the injured vessel (see Figure 4D).

BSDL may play a role in cancer-associated thrombosis. Even if a direct link between an increase in circulating BSDL (or BSDL stored in platelets) and a prothrombotic tendency is to date not known, pancreatic carcinoma is associated with a prothrombotic state (43). Furthermore, our laboratory has identified the protein FAPP as an oncofetal isoform of BSDL (40). Last, the concentration of circulating BSDL (including FAPP) is enhanced during the development of a pancreatic cancer (41). Together these results may identify BSDL and FAPP as important agents linking thrombosis to pancreatic carcinoma. These results may also suggest a role for the V3 loop of gp120 in thrombosis associated with HIV-1 infection (26). Further, we conclude that BSDL interaction with CXCR4 may be a new target for antithrombotic therapy in these and other disease states.

Methods

Mice. Wild-type C57BL/6J mice were obtained from The Jackson Laboratory. BSDL$^{-/-}$ mice were generously provided by J.L. Breslow and E.A. Fisher (The Rockefeller University, New York, New York, USA). BSDL-null mice have been previously described (34). The Beth Israel Deaconess Medical Center Institutional Animal Care and Use Committee approved all animal care and experimental procedures.

Antibodies and reagents. Affinity-purified rabbit polyclonal antibodies against the human pancreatic BSDL (referred to as pAbL64, pAbL32, and pAbantipeptide) were prepared at INSERM UMR-777 (30) and shown to cross-react with mBSDL. Irrelevant rabbit immunoglobulins were obtained from preimmune rabbit sera and purified by protein A–Sepharose affinity chromatography. A blocking monoclonal anti-human CXCR4 antibody (clone 44716.111) and CXCR4 inhibitor (AMD3100) were from Sigma-Aldrich. Rat monoclonal anti-mouse CD41 antibody (clone MWReg30), rat monoclonal anti-mouse P selectin antibody (clone RB 40.34), inhibitory mouse monoclonal anti-human CXCR4 antibody (clone 12G5), and PAC-1 FITC-labeled antibody directed against activated $\alpha_{IIb}\beta_3$ were from BD Biosciences — Pharmingen. Mouse anti-human fibrin II β-chain antibody (clone NYBT2G1) was from Accurate Chemical and Scientific Corp. Fab fragments from the anti-CD41 antibody were generated using the Immuno-Pure Fab Preparation Kit (Pierce Biotechnology) and then conjugated to Alexa Fluor 647 according to the manufacturer's instructions (Invitrogen). Anti-fibrin antibody was conjugated to Alexa Fluor 488. Human α-thrombin was from Hematologic Technologies Inc. A3P5P, MRS 2395 (P_2Y_{12} antagonists), MRS 2179 (P_2Y_1 antagonist), ADP, and SDF-1 were purchased from Sigma-Aldrich. AYPGKF peptide (TRAP-4) was from Anaspec. SFLLRN peptide (TRAP-1) and a peptide with the sequence of the V3-like loop of BSDL (17) were obtained from Eurogentec. The sequence-related peptide analogs of the V3-like loop (V3Lscr and V3Lsal) were generated by solid-phase peptide synthesis and their structures confirmed by automated Edman degradation on an ABI 891 Prosequencer (Applied Biosystems) and by mass spectroscopy.

Cell culture. HUVECs were isolated as described previously (44) and were obtained from F. Dignat-George (UMR-608 INSERM, Marseille, France). HUVECs were grown to confluence in EGM-2 medium and used at passages II–IV. HEK293t and CXCR4-transfected HEK293t cell lines were a generous gift from M. Biard-Piechaczyk (CNRS UMR 5121, Montpellier, France). HEK 293t-CXCR4 cells were maintained in DMEM medium supplemented with 10% FCS, penicillin (100 U/ml), streptomycin (100 μg/ml), zeomycin (0.25 mg/ml). HEK293t cell lines were cultured in DMEM without zeomycin. All these cells lines were kept at 37°C in a humidified atmosphere of 95% O_2 and 5% CO_2.

Platelet preparation. Human platelets were obtained from healthy volunteers who had not taken anti-platelet medications for 2 weeks prior to blood donation. Blood was drawn from healthy volunteers who provided informed consent. The procedure was performed according to a protocol approved by the Institutional Review Board of the Beth Israel Deaconess Medical Center. Platelets were separated from freshly drawn blood by centrifugation and washed twice in CGS (13 mM trisodium citrate, 30 mM dextrose, and 120 mM NaCl, pH 7.0) in the presence of 0.02 U/ml apyrase (Sigma-Aldrich) and 500 nM PGI_2 (Calbiochem) and once in ETS buffer (1 mM EDTA, 10 mM Tris-HCl, and 154 NaCl, pH 7.4) as described previously (45). Washed platelets were resuspended at a concentration of 3×10^8 platelets/ml in Tyrode buffer (138 mM NaCl, 2.9 mM KCl, 12 mM $NaHCO_3$, 5.5 mM glucose, 1.8 mM $CaCl_2$, and 0.4 mM $MgCl_2$, pH 7.4) containing 0.2% BSA (Sigma-Aldrich). Mouse platelets were prepared similarly and

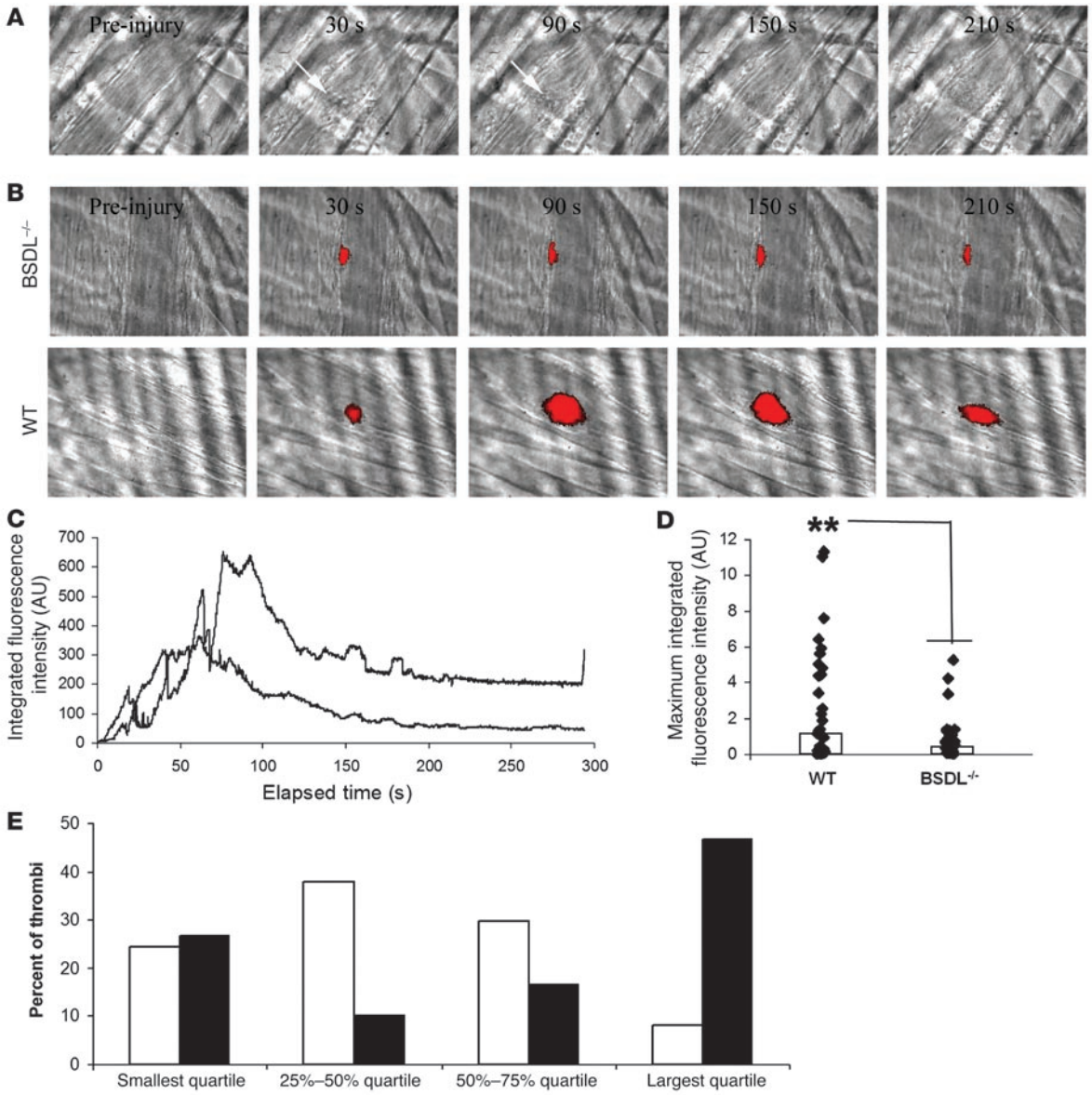

Figure 6

Thrombus formation is defective in BSDL-null mice. (**A**) Endogenous BSDL was not detected by pAbantipeptide (0.6 μg/g mouse) and Alexa Fluor 488–conjugated goat anti-rabbit IgG (0.6 μg/g mouse) in BSDL-null mice after a laser-induced injury. (**B**) Thrombus formation was studied after infusion of anti-CD41 antibody in BSDL-null (upper panel) or wild-type (lower panel) mice. Original magnification, ×600. (**C**) Median platelet integrated fluorescence intensity as a function of time (s) after a laser-induced injury to the arteriolar vessel wall in the mouse cremaster muscle. BSDL-null (lower curve) (BSDL$^{-/-}$; 36 thrombi, 3 mice) and wild-type (upper curve) (32 thrombi, 3 mice) mice were previously infused with Alexa Fluor 647–conjugated anti-mouse CD41 Fab fragment (0.25 μg/g mouse). (**D**) Maximum integrated fluorescence intensity during thrombus formation in wild-type (28 thrombi, 3 mice) and BSDL-null mice (30 thrombi, 3 mice) after laser-induced injury. The bars show the median value of the maximal fluorescence intensities. $^{**}P < 0.001$. (**E**) Quartile distribution of the maximum integrated fluorescence intensity associated with platelets during thrombus formation in BSDL-null (white bars) and wild-type (black bars) mice.

were resuspended at a concentration of 1×10^8 platelets/ml in Tyrode buffer containing 0.2% BSA. For the experiments monitoring calcium mobilization, mouse and human platelets were incubated with 3 μM fura-2/AM (Invitrogen) for 40 minutes in the dark at 37°C, pelleted, and resuspended in Tyrode buffer before use as previously described (38).

Prostacyclin enzyme immunoassay. HUVECs were seeded into a 24-well plate at 0.45×10^5 cells per well and maintained in EGM-2 medium. At 80% of confluence, HUVECs were incubated in medium 199 supplemented with inactivated FCS (5%) for 24 hours. BSDL in the presence and absence of thrombin in fresh medium 199 was added to HUVECs for 6 hours. Medium samples were centrifuged at 500 *g* for 5 minutes and stored at –80°C until assay. The concentration of keto-$PGF_{1\alpha}$, a metabolite of PGI_2, was assayed in medium samples by enzymatic immunoassay (Cayman Chemical Co.).

Nitric oxide assay. HUVECs were treated as described above. The concentration of nitric oxide was assayed in medium sample by colorimetric assay (Calbiochem).

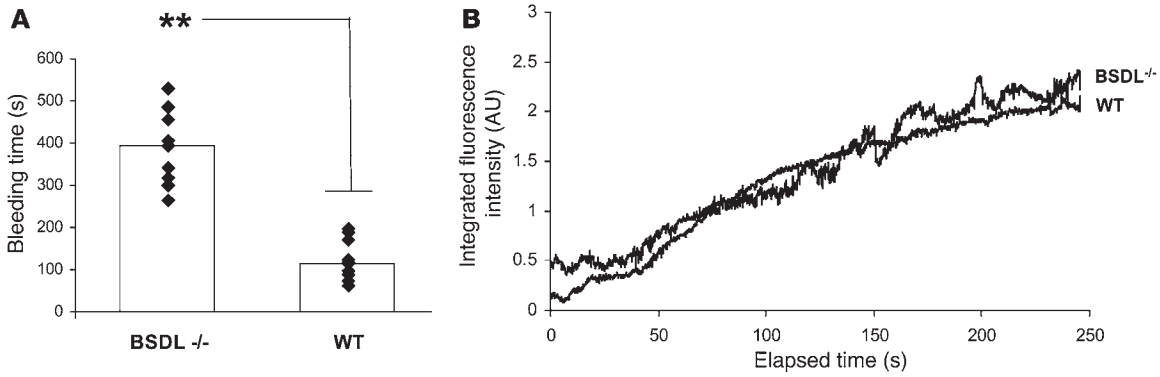

Figure 7
Thrombus formation but not fibrin generation is defective in BSDL-null mice in comparison with wild-type mice. (**A**) Bleeding time in seconds determined in BSDL-null (10 mice) and wild-type (10 mice) mice. Bars indicate median values; $^{**}P < 0.001$. (**B**) Median fibrin integrated fluorescence intensity in thrombi after laser-induced injury in wild-type (30 thrombi; 3 mice) and BSDL-null mice (28 thrombi; 3 mice). An Alexa Fluor 488–labeled monoclonal antibody specific for fibrin (0.4 μg/g mouse) was infused prior to laser injury.

PAGE and Western blotting. SDS-PAGE was performed on gels of polyacrylamide (7.5 % acrylamide) and 0.1 % sodium dodecyl sulfate as previously described (30).

Fluorescence microscopy. HUVECs and HEK293t and HEK293t-CXCR4 cells were grown to 80% confluence on microscope coverslips and washed 3 times with PBS buffer and fixed with 3% (vol/vol) paraformaldehyde for 20 minutes. The excess of paraformaldehyde was eliminated by washing the slides in 1 M glycine (pH 8.5). Between each step, cells were exhaustively rinsed with PBS. Cells were prepared for immunofluorescence as already described (42) using appropriate primary antibodies and conjugates. In some cases, resting or thrombin activated platelets (0.1 U/ml) were fixed with paraformaldehyde (3%) or glutaraldehyde (0.1%) for 30 minutes. Plate-

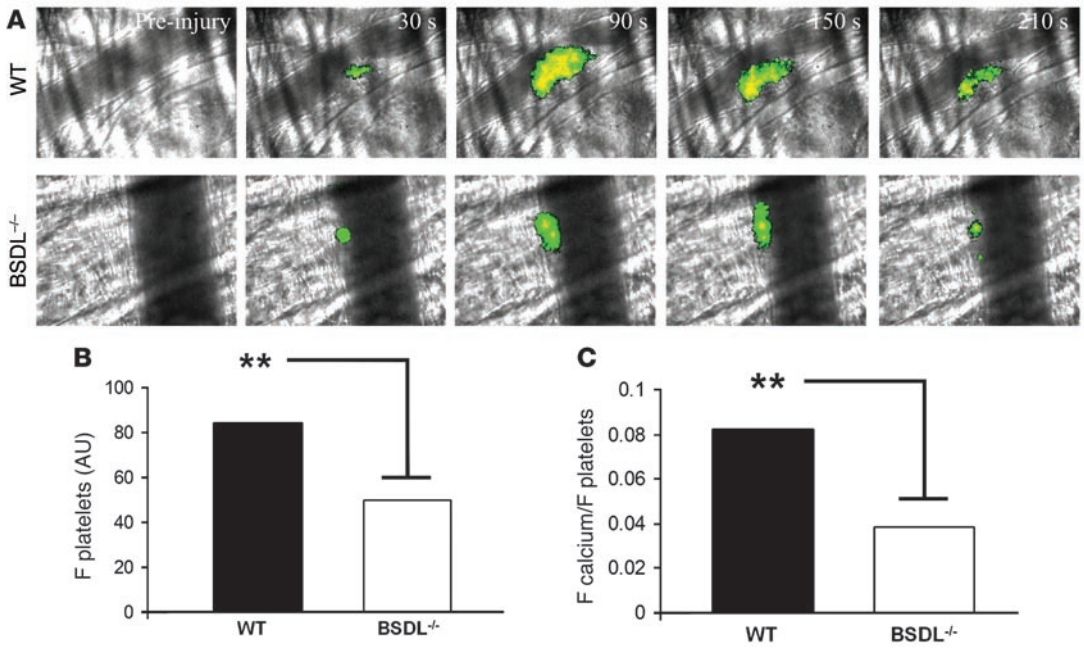

Figure 8
Platelet activation is defective in vivo in BSDL-null mice during thrombus formation. Platelets isolated from wild-type or BSDL$^{-/-}$ mice were loaded with fura-2/AM and infused into the circulation of mice of the same genotype as the donor mouse prior to laser-induced vessel wall injury. (**A**) Representative composite fluorescence and bright field images of thrombus formation showing fura-2–loaded platelet accumulation (green) and calcium mobilization (yellow) in wild-type (upper panel) and BSDL$^{-/-}$ mice (lower panel). Original magnification, ×600. (**B**) The bars indicate the median fluorescence intensity at 380 nm associated with platelet accumulation (F platelets) in wild-type mice (18 thrombi, 3 mice) and BSDL$^{-/-}$ mice (24 thrombi, 4 mice); $^{**}P < 0.001$. (**C**) To correct for thrombus size, the ratio of the fluorescence signals corresponding to platelet accumulation and calcium mobilization were compared using the ratios of the median integrated fluorescence intensity associated with calcium mobilization and the median integrated fluorescence intensity associated with platelets. The bars indicate the calcium mobilization per platelet (F calcium/F platelets) in wild-type and BSDL$^{-/-}$ mice. $^{**}P < 0.001$.

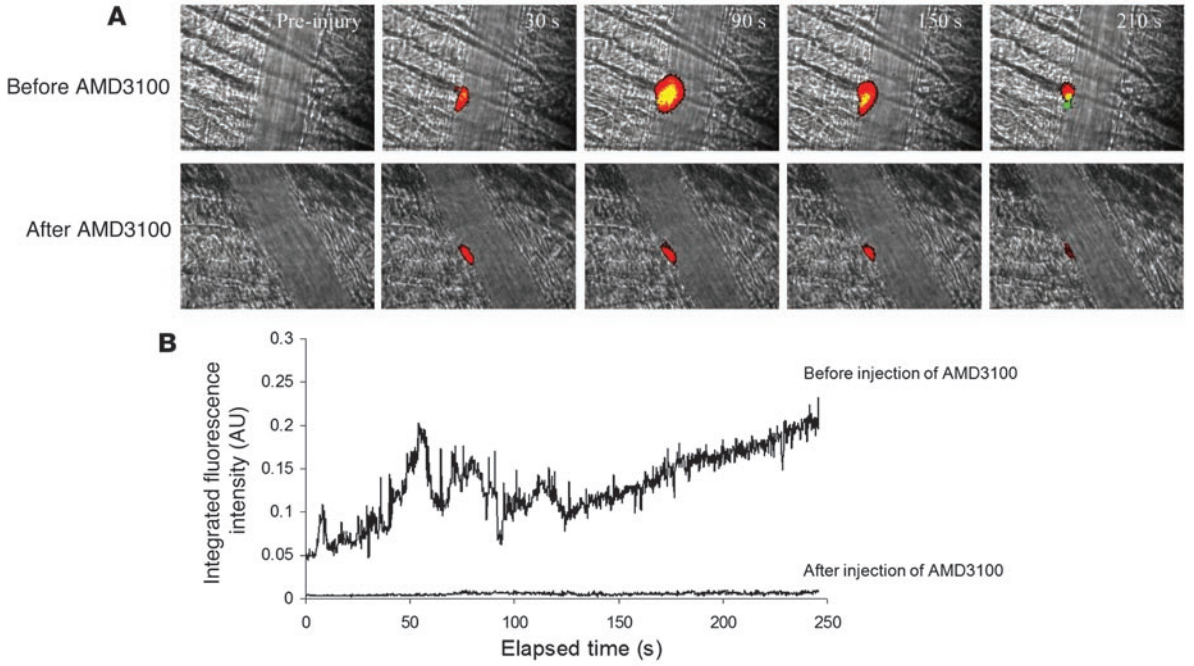

Figure 9
Involvement of CXCR4 in thrombus formation. Wild-type mice were infused with Alexa Fluor 647–conjugated anti-mouse CD41 Fab fragment (0.25 μg/g mouse), pAbantipeptide (0.6 μg/g mouse), and Alexa Fluor 488–conjugated goat anti-rabbit antibody (0.6 μg/g mouse) prior to injury. (**A**) Top row: Thrombus formation after laser injury in the absence of AMD3100. Bottom row: Thrombus formation after laser injury following infusion of AMD3100. Fluorescence signal of accumulated anti-CD41 antibody, red; fluorescence signal of accumulated pAbantipeptide, green; merge, yellow. Original magnification, ×600. (**B**) Median BSDL (pAbantipeptide) integrated fluorescence intensity in laser-induced thrombi in wild-type mice before and after treatment as in **A** with AMD3100 (1.25 μg/g mouse). For **A** and **B**, 30 thrombi in 3 wild-type mice were analyzed.

lets were then washed 3 times in CGS buffer and incubated for 2 hours with appropriated antibodies.

Flow cytometry. Flow cytometry experiments were performed on 1.5×10^7 washed human platelets. Resting or thrombin-activated (0.5 U/ml) platelets were incubated with or without hBSDL (5 μg) or V3-like loop peptides (1 μg) for 5 minutes, in the presence of 1 mM $CaCl_2$. For BSDL detection, platelets were permeabilized as indicated by addition of 0.01% saponin in all the buffers. Platelets were then incubated with antibodies against P selectin or activated $\alpha_{IIb}\beta_3$ or with the antibody pAbL32 coupled to Alexa Fluor 488 and directed against hBSDL. A secondary FITC-conjugated antibody was added when required. Expression of activated $\alpha_{IIb}\beta_3$, P selectin, or BSDL on the surface of and in resting and activated platelets was analyzed using a BD FACSCalibur flow cytometer.

Platelet aggregation studies. Washed human platelets (3×10^8/ml) were stirred at 37°C for 10 minutes in a 4-channel aggregometer (Chrono-Log Corp.). hBSDL (5 μg), V3-like peptides (1 μg), or SDF-1 (100 μM) were added to platelets after activation with thrombin (0.15–1 U/ml), TRAP-1 (10–15 μM), TRAP-4 (100 μM), or ADP (2.5–5 μM). In some experiments, hirudin (20 μg/ml), apyrase (0.4 U), A3P5P (34 μM), MRS2395 (10 μM), or MRS2179 (100 μM) was added. The extent of platelet aggregation was defined as the percentage change in optical density.

Platelet spreading. Thrombin-activated (1 U/ml) or resting platelets were incubated with hBSDL (5 μg) for 5 minutes and the platelets transferred to glass coverslips. After 5, 20, or 40 minutes, platelet spreading was stopped by the addition of paraformaldehyde (2%) for 20 minutes. The coverslips were washed with PBS and platelets bound to the coverslips were detected with Alexa Fluor 647–conjugated anti-mouse CD41 Fab fragment. Platelets attached to coverslips were washed 3 times with PBS to remove the excess of Alexa Fluor 647–conjugated anti-mouse CD41 Fab fragment. Coverslips were mounted on microscope slides, and fluorescent images were recorded and analyzed with Slidebook software (Intelligent Imaging Innovations).

In vitro calcium mobilization. Fura-2–loaded platelets (1×10^8 platelets/ml) were preincubated and stirred in a cuvette in a Perkin Elmer LS45 Fluorescence Spectrometer for 1 minute at 37°C with 2 mM of $CaCl_2$; then 0.1 U of thrombin, 0.1 μg of V3-like loop peptide, or 0.5 μg of hBSDL was added and the fluorescence change recorded. The fluorescence emission following excitation at 340 nm and 380 nm was recorded at 510 nm (36, 46).

Intravital microscopy. Intravital videomicroscopy of the cremaster muscle microcirculation was performed as previously described (29). Mice were preanesthetized with intraperitoneal ketamine (125 mg/kg; Abbott Laboratories), xylazine (12.5 mg/kg; Phoenix Pharmaceuticals), and atropine (0.25 mg/kg; American Pharmaceutical Partners). A tracheal tube was inserted and the mouse maintained at 37°C on a thermo-controlled rodent blanket. To maintain anesthesia, Nembutal (Abbott Laboratories) was administered through a cannulas placed in the jugular vein. After the scrotum was incised, the testicle and surrounding cremaster muscle were exteriorized onto an intravital microscopy tray. The cremaster preparation was superfused with thermo-controlled (36°C) and aerated (95% N_2, 5% CO_2) bicarbonate-buffered saline throughout the experiment. Microvessel data were obtained using an Olympus AX microscope with a 60× 0.9 NA water immersion objective. The fluorescence microscopy system has previously been described (47). Digital images were captured with a Cooke Sensicam CCD camera in 640 × 480–pixel format.

Laser-induced injury. Antibodies or exogenously labeled mouse platelets (250×10^6 to 300×10^6) were infused through the jugular vein into the circulation of an anesthetized mouse. Vessel wall injury was induced with

a nitrogen dye laser (Micropoint; Photonics Instruments) focused through the microscope objective, parfocal with the focal plane and aimed at the vessel wall (35). Typically 1 or 2 pulses were required to induce vessel wall injury. For the experiments involving injection through the jugular vein of antibodies against the endogenous BSDL (pAbL32, pAbL64, pAbantipeptide), against CD41, or against fibrin in the presence or absence of CXCR4 inhibitor (AMD3100), 3 or 4 mice were studied and a maximum of 10 thrombi induced per mouse. For the in vivo calcium experiments, mouse platelets loaded with fura-2 were injected in a mouse through the jugular vein. Six thrombi were generated per mouse over a time course of about 45 minutes. For this set of experiments, 3 mice were studied. In all experiments new thrombi were formed upstream of earlier thrombi to avoid any contribution from thrombi generated earlier. There were no characteristic trends in thrombus size or thrombus composition in sequential thrombi generated in a single mouse during an experiment. Image analysis was performed using Slidebook. Fluorescence data were captured digitally at up to 50 frames per second and analyzed as previously described (35).

Confocal intravital microscopy. Confocal intravital microscopy was performed as previously described (47), except that the rate of image acquisition was increased. A modified Lambda DG-4 (Sutter) was used to generate monochromatic light from a 3-line argon-krypton laser. For image analysis, the mean and maximal background intravessel fluorescence after excitation at 488 and 647 nm was defined as the average of the mean and maximal voxel fluorescence intensity in 20 neighboring sections of the vessel prior to laser-induced injury. This value was subtracted from the fluorescence signal.

Bleeding time assays. Mouse tail bleeding times were determined as previously described (48). The investigator was blinded to the genotype of the mice. Briefly, a 1- to 3-mm portion of the distal tail was removed from a 6- to 8-week-old mouse, the tail was immersed in isotonic saline (37°C), and the time to complete cessation of blood flow recorded. The bleeding time was monitored for a maximum of 10 minutes.

Statistics. The aggregation and spreading data were expressed as mean ± SD. Significance was determined by paired 2-tailed Student's *t* test for the in vitro experiments and Wilcoxon's rank-sum test for the in vivo experiments. The difference was considered significant at $P < 0.05$.

Acknowledgments

The authors are indebted to E.A. Fisher and J.L. Breslow (The Rockefeller University) for providing the BSDL-null mice. The authors are grateful to M. Jacob for the synthesis of V3Lscr and V3Lsal peptides, Nadine Bruneau for review of the original data on apolipoprotein-bound BSDL, Marie Christine Alessi for the use of the aggregometer, and Françoise Dignat-George for the gift of HUVECs. This work was supported by grants from the NIH and by institutional funding from INSERM and the Université de la Méditerranée.

Received for publication May 10, 2007, and accepted in revised form September 19, 2007.

Address correspondence to: Laurence Panicot-Dubois, INSERM UMR 911, 27 Bld. Jean Moulin, Faculté de Médecine — Timone, 13385 Marseille cedex 05, France. Phone: 33-491-324-400; Fax: 33-491-830-187; E-mail: lpdubois@medecine.univ-mrs.fr.

1. Shamir, R., Johnson, W.J., Zolfaghari, R., Lee, H.S., and Fisher, E.A. 1995. Role of bile salt-dependent cholesteryl ester hydrolase in the uptake of micellar cholesterol by intestinal cells. *Biochemistry.* **34**:6351–6358.
2. Howles, P.N., Carter, C.P., and Hui, D.Y. 1996. Dietary free and esterified cholesterol absorption in cholesterol esterase (bile salt-stimulated lipase) gene-targeted mice. *J. Biol. Chem.* **271**:7196–7202.
3. Lombardo, D. 2001. Bile salt-dependent lipase: its pathophysiological implications. *Biochim. Biophys. Acta.* **1533**:1–28.
4. Mas, E., Abouakil, N., Roudani, S., Franc, J.L., Montreuil, J., and Lombardo, D. 1993. Variation of the glycosylation of human pancreatic bile-salt-dependent lipase. *Eur. J. Biochem.* **216**:807–812.
5. Mas, E., Sadoulet, M.O., el Battari, A., and Lombardo, D. 1997. Glycosylation of bile salt-dependent lipase (cholesterol esterase). *Methods Enzymol.* **284**:340–353.
6. Hui, D.Y., and Howles, P.N. 2002. Carboxyl ester lipase: structure-function relationship and physiological role in lipoprotein metabolism and atherosclerosis. *J. Lipid Res.* **43**:2017–2030.
7. Bruneau, N., Bendayan, M., Gingras, D., Ghitescu, L., Levy, E., and Lombardo, D. 2003. Circulating bile salt-dependent lipase originates from the pancreas via intestinal transcytosis. *Gastroenterology.* **124**:470–480.
8. Bruneau, N., Richard, S., Silvy, F., Verine, A., and Lombardo, D. 2003. Lectin-like Ox-LDL receptor is expressed in human INT-407 intestinal cells: involvement in the transcytosis of pancreatic bile salt-dependent lipase. *Mol. Biol. Cell.* **14**:2861–2875.
9. Lombardo, D., et al. 1993. Is bile salt-dependent lipase concentration in serum of any help in pancreatic cancer diagnosis? *Pancreas.* **8**:581–588.
10. Blackberg, L., Blind, P.J., Ljungberg, B., and Hernell, O. 1985. On the source of bile salt-stimulated lipase in human milk: a study based on serum concentrations as determined by sandwich enzyme-linked immunosorbent assay technique. *J. Pediatr. Gastroenterol. Nutr.* **4**:441–445.
11. Shamir, R., et al. 1996. Pancreatic carboxyl ester lipase: a circulating enzyme that modifies normal and oxidized lipoproteins in vitro. *J. Clin. Invest.* **97**:1696–1704.
12. Blind, P.J., et al. 1991. Carboxylic ester hydrolase. A sensitive serum marker and indicator of severity of acute pancreatitis. *Int. J. Pancreatol.* **8**:65–73.
13. Auge, N., et al. 2003. Pancreatic bile salt-dependent lipase induces smooth muscle cells proliferation. *Circulation.* **108**:86–91.
14. Li, F., and Hui, D.Y. 1998. Synthesis and secretion of the pancreatic-type carboxyl ester lipase by human endothelial cells. *Biochem. J.* **329**:675–679.
15. Kodvawala, A., Ghering, A.B., Davidson, W.S., and Hui, D.Y. 2005. Carboxyl ester lipase expression in macrophages increases cholesteryl ester accumulation and promotes atherosclerosis. *J. Biol. Chem.* **280**:38592–38598.
16. Bosner, M.S., Gulick, T., Riley, D.J., Spilburg, C.A., and Lange, L.G., 3rd. 1988. Receptor-like function of heparin in the binding and uptake of neutral lipids. *Proc. Natl. Acad. Sci. U. S. A.* **85**:7438–7442.
17. Aubert-Jousset, E., et al. 2004. The combinatorial extension method reveals a sphingolipid binding domain on pancreatic bile salt-dependent lipase: role in secretion. *Structure.* **12**:1437–1447.
18. Rebai, O., Le Petit-Thevenin, J., Bruneau, N., Lombardo, D., and Verine, A. 2005. In vitro angiogenic effects of pancreatic bile salt-dependent lipase. *Arterioscler. Thromb. Vasc. Biol.* **25**:359–364.
19. Clemetson, K.J., et al. 2000. Functional expression of CCR1, CCR3, CCR4, and CXCR4 chemokine receptors on human platelets. *Blood.* **96**:4046–4054.
20. Klinger, M.H., et al. 1995. Immunocytochemical localization of the chemokines RANTES and MIP-1 alpha within human platelets and their release during storage. *Int. Arch. Allergy Immunol.* **107**:541–546.
21. Jin, D.K., et al. 2006. Cytokine-mediated deployment of SDF-1 induces revascularization through recruitment of CXCR4+ hemangiocytes. *Nat. Med.* **12**:557–567.
22. Kowalska, M.A., et al. 1999. Megakaryocyte precursors, megakaryocytes and platelets express the HIV co-receptor CXCR4 on their surface: determination of response to stromal-derived factor-1 by megakaryocytes and platelets. *Br. J. Haematol.* **104**:220–229.
23. Kowalska, M.A., et al. 2000. Stromal cell-derived factor-1 and macrophage-derived chemokine:2 chemokines that activate platelets. *Blood.* **96**:50–57.
24. Gear, A.R., et al. 2001. Adenosine diphosphate strongly potentiates the ability of the chemokines MDC, TARC, and SDF-1 to stimulate platelet function. *Blood.* **97**:937–945.
25. Gear, A.R., and Camerini, D. 2003. Platelet chemokines and chemokine receptors: linking hemostasis, inflammation, and host defense. *Microcirculation.* **10**:335–350.
26. Sakaida, H., et al. 1998. T-tropic human immunodeficiency virus type 1 (HIV-1)-derived V3 loop peptides directly bind to CXCR-4 and inhibit T-tropic HIV-1 infection. *J. Virol.* **72**:9763–9770.
27. Lombardo, D., Guy, O., and Figarella, C. 1978. Purification and characterization of a carboxyl ester hydrolase from human pancreatic juice. *Biochim. Biophys. Acta.* **527**:142–149.
28. De Clercq, E. 2005. Potential clinical applications of the CXCR4 antagonist bicyclam AMD3100. *Mini Rev. Med. Chem.* **5**:805–824.
29. Falati, S., Gross, P., Merrill-Skoloff, G., Furie, B.C., and Furie, B. 2002. Real-time in vivo imaging of platelets, tissue factor and fibrin during arterial thrombus formation in the mouse. *Nat. Med.* **8**:1175–1181.
30. Panicot-Dubois, L., et al. 2004. Monoclonal antibody 16D10 to the C-terminal domain of the feto-acinar pancreatic protein binds to membrane of human pancreatic tumoral SOJ-6 cells and inhibits the growth of tumor xenografts. *Neoplasia.* **6**:713–724.
31. Sim, D.S., Merrill-Skoloff, G., Furie, B.C., Furie, B., and Flaumenhaft, R. 2004. Initial accumulation of platelets during arterial thrombus formation in vivo is inhibited by elevation of basal cAMP levels. *Blood.* **103**:2127–2134.

32. Chou, J., Mackman, N., Merrill-Skoloff, G., Pedersen, B., Furie, B.C., and Furie, B. 2004. Hematopoietic cell-derived microparticle tissue factor contributes to fibrin formation during thrombus propagation. *Blood.* **104**:3190–3197.
33. Tran, J., et al. 2002. A role for survivin in chemoresistance of endothelial cells mediated by VEGF. *Proc. Natl. Acad. Sci. U. S. A.* **99**:4349–4354.
34. Weng, W., et al. 1999. Intestinal absorption of dietary cholesteryl ester is decreased but retinyl ester absorption is normal in carboxyl ester lipase knockout mice. *Biochemistry.* **38**:4143–4149.
35. Dubois, C., Panicot-Dubois, L., Merrill-Skoloff, G., Furie, B., and Furie, B.C. 2006. Glycoprotein VI-dependent and -independent pathways of thrombus formation in vivo. *Blood.* **107**:3902–3906.
36. Dubois, C., Atkinson, B., Furie, B.C., and Furie, B. 2006. Real time in vivo imaging of platelets during thrombus formation. In *Platelets.* 2nd edition. A.D. Michelson, editor. Elsevier/Academic Press. Worcester, Massachusetts, USA. 611–628.
37. Dubois, C., Panicot-Dubois, L., Furie, B.C., and Furie, B. 2004. Direct real time visualization of platelet calcium signaling in vivo: role of platelet activation and thrombus formation in a living mouse [abstract]. *Blood (ASH Annual Meeting Abstracts).* **104**:325.
38. Dubois, C., Panicot-Dubois, L., Gainor, J.F., Furie, B.C., and Furie, B. 2007. Thrombin-initiated platelet activation in vivo is von Willebrand factor-independent during thrombus formation. *J. Clin. Invest.* **117**:953–960. doi:10.1172/JCI30537.
39. Khorana, A.A., and Fine, R.L. 2004. Pancreatic cancer and thromboembolic disease. *Lancet Oncol.* **5**:655–663.
40. Mas, E., et al. 1993. Human fetoacinar pancreatic protein: an oncofetal glycoform of the normally secreted pancreatic bile-salt-dependent lipase. *Biochem. J.* **289**:609–615.
41. Fujii, Y., Albers, G.H., Carre-Llopis, A., and Escribano, M.J. 1987. The diagnostic value of the foetoacinar pancreatic (FAP) protein in cancer of the pancreas; a comparative study with CA19/9. *Br. J. Cancer.* **56**:495–500.
42. Pasqualini, E., et al. 1998. Molecular cloning of the oncofetal isoform of the human pancreatic bile salt-dependent lipase. *J. Biol. Chem.* **273**:28208–28218.
43. Khorana, A.A. 2003. Malignancy, thrombosis and Trousseau: the case for an eponym. *J. Thromb. Haemost.* **1**:2463–2465.
44. Jaffe, E.A., Nachman, R.L., Becker, C.G., and Minick, C.R. 1973. Culture of human endothelial cells derived from umbilical veins. Identification by morphologic and immunologic criteria. *J. Clin. Invest.* **52**:2745–2756.
45. Fox, J.E., Reynolds, C.C., and Boyles, J.K. 1992. Studying the platelet cytoskeleton in Triton X-100 lysates. *Methods Enzymol.* **215**:42–58.
46. Dubois, C., Panicot-Dubois, L., Furie, B.C., and Furie, B. 2005. Dynamics of calcium mobilization in platelets during thrombus formation in a living mouse [abstract]. *Blood (ASH Annual Meeting Abstracts).* **106**:649.
47. Celi, A., et al. 2003. Thrombus formation: direct real-time observation and digital analysis of thrombus assembly in a living mouse by confocal and widefield intravital microscopy. *J. Thromb. Haemost.* **1**:60–68.
48. Kato, K., et al. 2004. Genetic deletion of mouse platelet glycoprotein Ibbeta produces a Bernard-Soulier phenotype with increased alpha-granule size. *Blood.* **104**:2339–2344.